NOW LIVE!
connect.aium.org

The association for medical ultrasound
aium®
AMERICAN INSTITUTE OF ULTRASOUND IN MEDICINE

THE AIUM'S ONLINE COMMUNITY
Connect

New benefit for AIUM members!

aium | connect

AIUM Connect brings together multidisciplinary professionals in an online space to foster collaboration in an effort to advance the safe and effective use of medical ultrasound.

Share ideas, provide insight, and receive feedback through thought-provoking discussions and resource sharing in an easily accessible web-based platform.

Empowering individuals to partner with others strengthens the future of ultrasound in medicine and leads to improved patient care. To join the conversation, visit **connect.aium.org**.

NEW AIUM Connect is a new benefit for members!
To join the AIUM, visit **aium.org/join/renew**.

NOW LIVE

AIUM Connect is now live!
To join the conversation,
visit **connect.aium.org**.

About the AIUM in 30 Seconds: The American Institute of Ultrasound in Medicine (AIUM) is a multi-disciplinary network of nearly 10,000 professionals who are committed to advancing the safe and effective use of ultrasound in medicine.

FOLLOW US ONLINE

American Institute of Ultrasound in Medicine (AIUM) | 14750 Sweitzer Ln, Suite 100 | Laurel, MD 20707 | **aium.org** | 800-638-5352

Quantitative Ultrasound and the Pancreas: Demonstration of Early Detection Capability

Rita J. Miller, DVM, Aiguo Han, PhD, John W. Erdman Jr PhD, Matthew A. Wallig, DVM, PhD, William D. O'Brien Jr PhD

Received May 7, 2018, from the Bioacoustics Research Laboratory, Department of Electrical and Computer Engineering (R.J.M., A.H., W. D.O.); Department of Food Science and Human Nutrition (J.W.E.), and Department of Pathobiology (M.A.W.), University of Illinois at Urbana-Champaign, Urbana, Illinois, USA. Manuscript accepted for publication November 5, 2018.

This work was supported in part by the National Institutes of Health (R37EB002641).

The authors thank Jamie R. Kelly and Jake Berndt for their valued assistance. We also thank the University of Illinois Veterinary Diagnostic Laboratory.

Address correspondence to William D. O'Brien Jr, PhD, Bioacoustics Research Laboratory, Department of Electrical and Computer Engineering, University of Illinois at Urbana-Champaign, 306 North Wright Street, Urbana, IL 61801 USA.

E-mail: wdo@uiuc.edu

Abbreviations

AC, attenuation coefficient; BSC, backscatter coefficient; CCK, cholecystokinin; FOI, field of interest; QUS, quantitative ultrasound; RF, radio frequency; subROIs, subregions of interest

doi:10.1002/jum.14901

Objectives—To show that quantitative ultrasound biomarkers attenuation (AC) and backscatter (BSC) coefficients are effective tools to detect early changes in acute pancreatitis, using a cerulein-induced pancreatitis rat model.

Methods—Sprague-Dawley rats (n = 68) were divided into 8 groups: uninjected cage controls, saline-injected controls, and cerulein-injected rats euthanized at 2, 4, 15, 24, 48, and 60 hours after injection. Pancreatic AC and BSC (25–55 MHz) were estimated in vivo (Vevo 2100, VisualSonics, Toronto, CA) and ex vivo (40-MHz transducer). The pancreas of each rat was evaluated histopathologically.

Results—Changes in both in vivo and ex vivo AC and BSC relative to controls reflected temporal histomorphologic changes. Overall, there were decreased AC and BSC at early time points and then rebound toward control values over time. Maximal in vivo AC and BSC decreases occurred at 2 hours after cerulein injection. Attenuation coefficient changes corresponded well with early pancreatic edema and acinar cell vacuolation, with rebound as edema decreased, autophagy/cellular death occurred, and histiocytic infiltrates and fibrosis manifested. Backscatter coefficient decreased early but rebounded as autophagy and apoptosis increased, only to fall as acinar atrophy peaked, and fibrosis and histiocytic infiltration increased.

Conclusions—Cerulein-induced pancreatitis is an excellent model for studying ultrasonic AC and BSC biomarkers during the early stages of acute pancreatitits, reflecting microscopic structural changes. Edema followed by cell shrinkage and apoptosis, then histiocytic infiltration and fibrosis, has certain similarities with the morphologies of some forms of pancreatic carcinoma. This suggests that quantitative ultrasound may be very useful for early detection of disease onset or response to therapy for not only acute pancreatitis but also pancreatic cancer.

Key Words—attenuation coefficient (AC); backscatter coefficient (BSC); cerulein; early detection; pancreatitis; quantitative ultrasound

Pancreatitis, which is inflammation of the pancreas, can occur as the result of inappropriate activation of digestive enzymes while still within the pancreatic acinar cell. This excessive activation results in acinar cell injury and death, with leakage of released active enzymes into surrounding tissues, exacerbating and expanding the damage, leading to serious clinical disease. Acute pancreatitis is common, although most patients recover without hospitalization. However, a significant number of patients (approximately 20%) progress to severe clinical disease that can

be life threatening.[1] The most common presenting complaints are upper abdominal pain, nausea, and vomiting, which can be associated with other diseases as well, such as gastritis and cholangitis. In the United States, acute pancreatitis is the number one gastrointestinal diagnosis and the 21st overall diagnosis of hospital admissions (approximately 274,000 annually), resulting in an annual cost of about $2.6 billion. Between 2000 and 2009 there was a 30% increase in hospital admissions for suspected acute pancreatitis in the United States. The number of deaths with pancreatitis as the underlying cause is approximately 1 in 100,000.[2] Deaths in acute pancreatitis are typically due to a systemic inflammatory response resulting in organ failure or sepsis.[1] Acute pancreatitis creates both a financial and physical health burden; therefore, diagnosing patients early is critical to achieving the best potential outcome in therapeutic interventions.

Pancreatic cancer has a low incidence but high fatality rate, with only an 8% 5-year survival rate. Pancreatic cancer incidence (approximately 12 per 100,000) and number of deaths (approximately 11 per 100,000) have stayed more or less the same over time.[2–4] According to the American Cancer Society, 55,440 new cases will be diagnosed in 2018 (representing about 3% of all cancers in the United States) and 44,330 people will die in 2018 (representing about 7% of all cancers in the United States) due to pancreatic cancer.[5] In 2004, pancreatic cancer costs in the United States were $4.3 billion (second highest of all digestive cancers).[6] In the United States, of the number of new cancer cases and cancer deaths in 2017, pancreatic cancer ranks as number 12 and number 3, respectively.[3] Unfortunately, pancreatic cancer is often not detected until it is at an advanced stage, resulting in a short life expectancy.

The pancreas is both an exocrine and an endocrine gland. The exocrine portion makes up the majority of pancreatic tissue (85%). Acinar cells, the major cell type within the exocrine pancreas, synthesize, store, and secrete essential enzymes (proteases, lipases, amylases) that catalyze the digestion of protein, fat, and carbohydrates within the small intestine. The enzymes are secreted, still in an inactive state, into the pancreatic ducts, together with bicarbonate-rich secretory fluids produced by duct cells themselves. The pancreatic ducts carrying the enzyme-rich fluid eventually coalesce into 1 or 2 main ducts that empty into the duodenum, where the secreted enzymes are activated, near or at the entry point for the main biliary duct from the liver. The endocrine pancreas, on the other hand, is composed of islets that make and secrete metabolic hormones such as insulin and glucagon, directly into the bloodstream. In this study, we are concerned with the exocrine pancreas. Pancreatic acinar cells (pyramid shaped with the apical [luminal] portion being narrower than the base) produce inactive digestive enzyme precursors (zymogens) that are packaged into membrane-bound granules to prevent premature activation, thus protecting the pancreas from autodigestion. "Recycling" of unused zymogen is highly regulated for the protection of the acinar cell. When signaling mechanisms for secretion are excessive, flawed, or inappropriate, such that abnormal "trafficking" of zymogen granules occurs, the protective mechanisms break down and these enzymes can become activated within the acinar cell, resulting in a variety of responses – vacuolation and autophagy followed by apoptosis, necroptosis, or necrosis – leading to pancreatitis.[7]

Grossly, the pancreas in the rat is divided into 3 regions: splenic, gastric, and a rather dispersed duodenal portion. It is a loosely aggregated organ with a thin, transparent capsule, extending from the underside of the spleen, along the greater curvature of the stomach, and along the proximal duodenum (distributed in small clusters within the mesentery). It is pale pink in color and slightly thicker and more solid than the surrounding omental and mesenteric adipose tissue.

Diagnostic advances are needed to develop a quick, noninvasive, relatively easy, and inexpensive technique for diagnosing and assessing early-onset pancreatitis and, as an added application, the very early invasive stages of pancreatic cancer in which inflammation and initial stromal changes prior to invasion and population of new sites by neoplastic pancreatic cells mirror some of the same changes observed in pancreatitis.[8,9] Understanding the progression of acute pancreatitis is imperative for successful intervention and treatment before hospitalization occurs. Most patients, by the time they present to the emergency room or hospital, have already gone through the early stages of the disease. Early detection would aid in preventing potentially

irreversible and life-threatening effects on the pancreas.

In this study, quantitative ultrasound (QUS), together with histopathologic evaluation in which severity scoring of various changes typical of pancreatitis was performed, were exploited to investigate the possibility that ultrasound might be a useful diagnostic tool in assessing the early stages of this disease. To accomplish this, we used a cerulein-induced rat model of acute pancreatitis[10] and monitored the course of the disease over a 60-hour (2.5-day) duration. We estimated in vivo and ex vivo the QUS biomarkers, backscatter coefficient (BSC) and attenuation coefficient (AC), and scored various markers of acinar cell injury and pancreatic inflammation by histopathology.[11,12]

Cerulein-induced acute pancreatitis is a well-studied model characterized by a mild self-limiting, low-mortality pancreatitis[11] that allows for regeneration of the pancreas in approximately 7 days after cerulein administration has ceased. Cerulein, discovered and extracted from the skin of Australian green tree frogs,[13] is similar in action to the pancreatic stimulatory hormone cholecystokinin (CCK). Cholecystokinin, secreted by specialized duodenal cells when gastric content enters the duodenal lumen, together with vagal stimulation is responsible for secretion of zymogen granules from acinar cells into pancreatic ductular lumens. The 5 peptides (Gly-Trp-Met-Asp-Phe) at the carboxy-terminus are the same in both CCK and cerulein, and both contain a sulfated tyrosine at the same location. Like CCK, cerulein stimulates pancreatic and gastric secretions by binding to CCK receptors on the acinar cells. The natural sulfated version of cerulein, compared to the nonsulfated version, is far more effective in stimulating dose-dependent pancreatic secretions than CCK.[14]

Administration of cerulein at a supramaximal dose (level above that which produces maximal secretion) results in less pancreatic secretion leaving the pancreas and an accumulation of digestive enzymes within the acinar cells. Zymogen granules "line up" at the apical end of the acinar cell, but secretory capacity is saturated.[15] Zymogen is redirected to lysosomes for degradation (microautophagy). In severe cases, the lysosomes may expand to very large sizes, which manifests morphologically as vacuolation.[16] Lysosomal "overload" soon ensues, and activation of lysosomal enzymes that enhance activation of zymogens, rather than neutralize them, may occur. If zymogens become prematurely activated within an acinar cell, causing damage to surrounding cellular organelles, "macroautophagy," also known simply as "autophagy," will occur,[17] with sequestration of entire portions of membrane-bound cytoplasm within large autophagic vacuoles that then fuse with lysosomes. If this is insufficient, then there may be shrinkage and apoptosis of the affected acinar cell; resident macrophages (histiocytes) or macrophages recruited from the bloodstream will then ingest the membrane-bound apoptotic bodies. If damage is sufficiently severe that apoptotic pathways are disrupted, the cell will rupture and die in an uncontrolled fashion (necroptosis or single-cell necrosis) and spillage of cellular content, including activated zymogens, will happen. This leads to digestion of the pancreas and results in widespread uncontrolled cell death affecting entire acini or lobules (necrosis). The remaining acinar cells, devoid of zymogen, initially shrink and "dedifferentiate," as a prelude to replacement of lost acinar cells via mitosis and subsequent repopulation of the regenerated cells by newly synthesized zymogen granules. Often in this model, virtually complete regeneration of the pancreas to near normal can occur within 7 days. The aforementioned morphologic changes (vacuolation, autophagy, apoptosis, and necroptosis as well as inflammatory edema, inflammation cell infiltrate, and fibrosis [in severe cases]) can be identified and assessed via histologic examination. In the cerulein model of pancreatitis, in particular the rat, the pancreatitis is self-limiting and is characterized by profound early interstitial edema, apoptosis predominant over necrosis, histiocytic infiltration, sparse influx of neutrophils, minimal fibrosis, and virtually complete recovery to normal by 7 days.[18]

This minimally invasive model has been induced in rats,[11] mice,[11] hamsters,[19] and dogs.[20] The rat model provides an adequate amount of pancreatic tissue for both QUS and histologic assessment and in many ways resembles the early stages of human acute pancreatitis.[21] Further, the edematous stroma and shrinkage and dedifferentiation of acinar cells due to loss and impaired production of zymogen granules[22] has certain similarities with the altered stroma and dedifferentiated morphology of neoplastic acinar cells in some forms of pancreatic carcinoma. Therefore, the rat model is appropriate for evaluating the potential of QUS early detection capability for not only

acute pancreatitis but also the early invasive stages of pancreatic cancer as well.

Materials and Methods

Animal Protocol

The experimental animal protocol was approved by the Institutional Animal Care and Use Committee of the University of Illinois at Urbana-Champaign and satisfied all campus and National Institutes of Health rules for the humane use of laboratory animals. Animals were housed in an Association for Assessment and Accreditation of Laboratory Animal Care–approved animal facility and provided food and water ad libitum.

For injection, sulfated cerulein was purchased from Fisher Scientific (Alpha Aesar, Ward Hill, MA; cat #AAJ64320MCR). The 1-g vial of white powder was kept at –20°C until needed, brought up to room temperature before diluting to make aliquots, and spun down to ensure all the powder was at the bottom of the vial. For use, a 10-mL stock (100 μg/mL) using room temperature sterile 0.9% NaCl as diluent was prepared, ensuring that the cerulein was completely dissolved by initially vortexing and then pipetting up and down. From the stock, 0.5-mL aliquots were prepared and kept stored at –20°C until needed.

On the day of injections, the number of aliquots required to inject the requisite number of rats for that day were brought to room temperature. Based on the weight of the rat that day, the amount of cerulein required for 4 doses of 40 μg/kg each for each rat was calculated and the solution diluted such that 100 μL was administered at each of the hourly injections.

Sixty-eight female Sprague-Dawley rats were purchased from Envigo (Indianapolis, IN). At the time of injection they were 12.5 to 16.0 weeks of age with an average body weight of 228 g. The rats were divided into 8 scanning groups; cage control (no cerulein or saline injected), saline control (saline injected), and 2-hour, 4-hour, 15-hour, 24-hour, 48-hour, and 60-hour post-cerulein injection. Except for the 2 control groups, each unanesthetized rat received 40 μg/kg of sulfated cerulein injected intraperitoneally hourly 4 times.[10] The cage control group received no injections. The saline control group received 100 μL of sterile saline injected intraperitoneally hourly 4 times; the rats were euthanized 2 hours after the last saline injection. Rats were monitored between injections and for a minimum of 15 minutes after the last injection, and then returned to the animal facility until time of scanning. No evidence of abdominal pain or any other clinical signs from the cerulein injections were seen over the course of this study.

In vivo QUS Imaging

Each rat was anesthetized with 5% isoflurane at an oxygen flow rate of 2 L/min and maintained at 2% isoflurane (or to effect) at an oxygen flow rate of 2 L/min; the rat was then weighed and ophthalmic ointment was applied, and then the rat was placed in a supine position on the physiologic monitoring table of the 2100 system (Vevo 2100; VisualSonics, Toronto, CA), which has a warming pad with monitoring of respiratory and heart rates. The abdomen was shaved, depilated, and cleaned with alcohol. Pedal reflex was tested prior to surgery to ensure that a surgical plane of anesthesia was present. To expose the pancreas, an approximate 2-cm abdominal incision was made left of midline distal to the ribs using iris scissors. Forceps were used to gently lift and exteriorize the pancreas and spleen. The dorsal surface of the spleen was placed on Plexiglas positioned adjacent to the rat, so that the spleen was perpendicular to the body and the pancreas was on top of the spleen. This allowed the visualization of the pancreas tissue on top of the spleen. The pancreas is hyperechoic to the surrounding spleen (Figure 1).

Using degassed ultrasound gel that was applied to the pancreas, radio frequency (RF) data for AC and BSC estimates were acquired using the MS-550S (25–38 MHz) transducer (positioned perpendicular to the body and parallel to the pancreatic tissue), which was connected to a 3-dimensional motor (positioned parallel to the body and perpendicular to the pancreatic tissue) attached to the 2100 positioning system. The 3-dimensional motor was used to collect 11 frames, 0.5-mm apart, in a caudal to cranial direction. After pancreas data collection, the ultrasound gel was removed, and a frame of data was collected from a calibrated reference phantom with known AC and BSC. After phantom data collection, the pancreas

and spleen were gently placed back into the abdominal cavity. A gauze pad soaked in 0.9% NaCl was placed over the surgery incision to keep the tissues inside the abdominal cavity to prevent drying during euthanasia. While still anesthetized, the rat was euthanized via CO_2.

The in vivo AC and BSC were derived from the acquired RF data of the pancreas and phantom by using the reference phantom technique.[23] The comprehensive implementation details are documented in work by Han et al[24] and briefly summarized as follows. Attenuation coefficient and BSC processing were performed using custom software programmed in MATLAB (The MathWorks, Natick, MA). A field of interest (FOI) outlining the pancreas boundary was drawn on the reconstructed B-mode image. The FOI was subdivided into overlapping rectangular subregions of interest (sub-ROIs) for in vivo AC processing. Each AC sub-ROI (size, 1 mm axial length × 1.1 mm lateral length) yielded an AC estimate computed using the spectral difference method. The AC estimates from all AC sub-ROIs were averaged to yield the mean AC estimate for the entire FOI. To estimate the in vivo BSC, the same FOI was redivided into overlapping rectangular BSC sub-ROIs (size, 0.77×0.77 mm^2), each of which yielded a BSC estimate, and the BSC estimates from all sub-ROIs were averaged to yield the mean BSC estimate for the entire FOI. The attenuation effect was compensated for during BSC calculation.

Figure 1. Example of an in vivo image of a normal rat pancreas, lying on top of the spleen, taken with the VisualSonics Vevo2100 system using the MS-550S transducer. The pancreas is hyperechoic to the surrounding spleen.

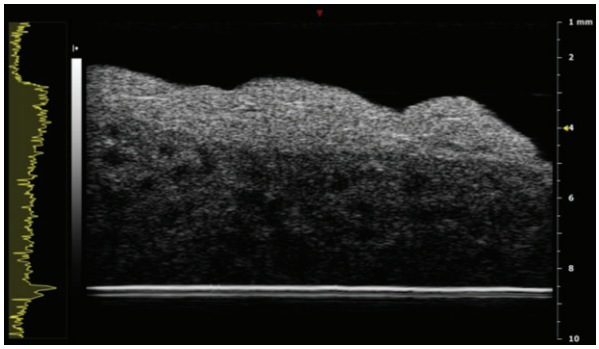

Ex vivo QUS Imaging

Immediately after euthanasia, the pancreas was removed en masse and weighed (Table 1). The surgery incision was enlarged using iris scissors and forceps. To avoid manipulation and subsequent damage of the pancreatic tissue, it was removed by holding the stomach and duodenum in one hand, stretching out the pancreatic tissue, and cutting the tissue away with the other. In addition, forceps were used to elevate the spleen to remove the attached pancreatic tissue. The entire pancreas was then gently lifted from below to place it on the dissecting table. Care was taken whenever handling the pancreatic tissue to preserve the integrity of the tissue for histologic analysis. A piece of pancreatic tissue no thicker than 2 mm was removed from the splenic region for ex vivo QUS scanning. It was placed in degassed 0.9% NaCl for transport to the scanning station. Sections from the splenic and gastric regions were trimmed and placed in tissue processing cassettes on a foam biopsy pad and fixed in 10% neutral buffered formalin for subsequent histopathologic evaluation (see below).

The ex vivo pancreatic tissue was ultrasonically scanned with a single-element 40-MHz focused transducer (25–55 MHz; f-number, 3; National Institutes of Health High-Frequency Transducer Resource Center, University of Southern California, Los Angeles, CA). The transducer was connected to a UTEX UT340 pulser/receiver (UTEX Scientific Instruments Inc, Mississauga, Ontario, CA) and moved via a computer-controlled positioning system (Daedal Parker Hannifin Corp, Irwin, PA). The pancreatic tissue was placed on Plexiglas within a tank filled with room temperature degassed 0.9% NaCl.

The ex vivo AC and BSC were obtained by using a through-transmission technique in the pulse-echo mode[25]

Table 1. Average Total Wet Weight of Pancreas

Time Point (h)	Weight of Entire Pancreas (g)
2	2.63
4	2.40
15	1.56
24	1.31
48	1.09
60	0.93
Cage control	1.36
Saline control	1.20

and a planar reference method,[26] respectively. The comprehensive implementation details are documented in work by Han et al[24] and briefly summarized as follows. The ex vivo AC was computed by comparing the echo signals from the Plexiglas with and without the pancreas tissue placed in the acoustic path. The ex vivo BSC was computed by using the same MATLAB software that was used for in vivo BSC processing. An FOI was drawn and subdivided into overlapping rectangular sub-ROIs (size, 0.56×0.56 mm^2) to compute the BSC; the instrumentation effects were removed by comparing the RF data from the pancreas in a sub-ROI to the RF data from the Plexiglas surface acquired at the same depth.[26] The BSC estimates from all sub-ROIs were averaged to yield the mean ex vivo BSC estimate for the entire FOI. The attenuation effect was compensated for during ex vivo BSC calculation.

Figure 2. In vivo mean AC and mean BSC estimates versus frequency for the pancreas in a rat model of cerulein-induced pancreatitis. Control = cage control. Saline = saline control. The numbers in parentheses represent the number of pancreases. AC, attenuation coefficient; BSC, backscatter coefficient.

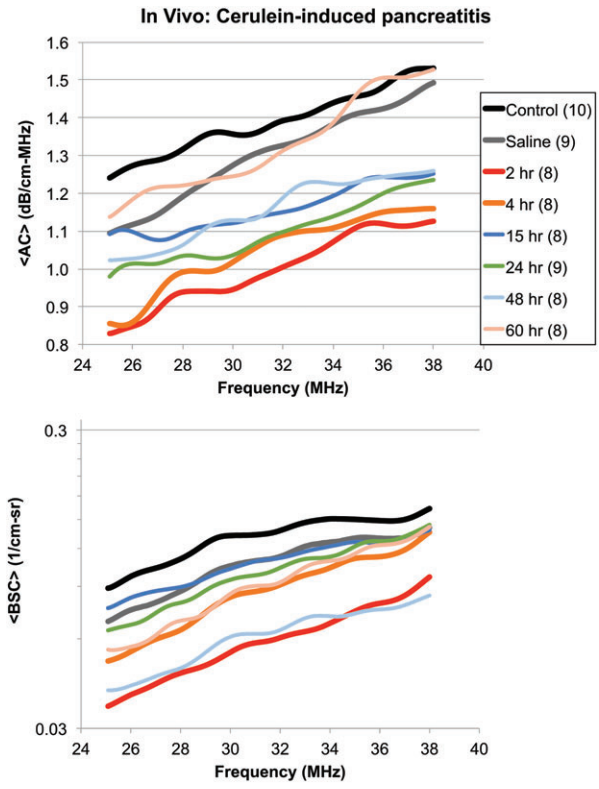

Histology

The pancreas was fixed in 10% neutral buffered formalin for 24 to 48 hours, prior to processing. Tissues were dehydrated in graded alcohols followed by xylene, then infiltrated by and embedded in paraffin, sectioned at 3 μm, mounted on a glass slide, and stained with hematoxylin and eosin for histopathologic evaluation by a board-certified veterinary pathologist (M.A.W.).

For a semiquantitative assessment of the changes over time, an expanded lesion scoring protocol ranging from 0 to 4, or 0 to 5 (the higher the value the more severe), modified from that of Usborne et al[12] was developed for each of 9 histologic parameters: zymogen depletion, acinar atrophy (decreased acinar size, both numerical and quantitative), acinar cell vacuolation, autophagic vacuoles, apoptotic bodies, interstitial edema, histiocyte infiltration, neutrophil infiltration, and fibrosis.

Results and Discussion

Quantitative Ultrasound Imaging

Both the BSC and AC were estimated in vivo and ex vivo for the pancreas in this rat model of cerulein-induced pancreatitis. The in vivo AC estimates versus frequency are shown in Figure 2. There is a clear separation into 2 QUS groupings. The first group has a higher AC and includes the controls (cage and saline) as well as the 60-hour post-cerulein time point. The second group shows a drop in AC and includes the 2-hour, 4-hour, 15-hour, 24-hour, and 48-hour post-cerulein time points. The 60-hour post-cerulein time points are trending back to the same level as the cage control and saline control rats. Pancreases from the 2-hour and 4-hour post-cerulein time points exhibited the largest drop in AC compared to the controls (cage and saline), indicating the ability of QUS to detect early changes. The in vivo BSC estimates versus frequency are also shown in Figure 2. At all time points BSC decreased to some extent compared to the controls (cage and saline). The 4-hour post-cerulein time point shows a large decrease compared to the controls, with the 2-hour post-cerulein time point having the largest drop. These results again demonstrate the ability to detect early changes following cerulein treatment. The 48-hour post-cerulein

time point also has a large drop in BSC compared to the controls. There was a clear separation between the 2 clustered 2-hour and 48-hour post-cerulein time points and the other 6 time points.

Ex vivo AC estimates versus frequency are shown in Figure 3. There was a drop in pancreatic AC compared to controls (cage and saline) at all post-cerulein time points, with the 2-hour post-cerulein time point exhibiting the largest drop in AC, again indicating the ability of QUS to detect very early changes. The ex vivo BSC estimates versus frequency are shown in Figure 3. At all time points there was a decrease to varying extents compared to the controls (cage and saline), except between 45 and 55 MHz, where pancreas from the 2-hour, 4-hour, and 15-hour post-cerulein time points had a higher BSC compared to the controls. The 24-hour, 48-hour, and 60-hour post-cerulein time points were clustered together, with the 48-hour post-cerulein time point exhibiting the largest drop in BSC.

Comparing the in vivo and ex vivo AC, the in vivo ACs tended to be higher over the same frequency range. Comparing in vivo and ex vivo BSC, the in vivo BSCs tended to be lower over the same frequency range. The bar graph in Figure 4 shows both the in vivo and ex vivo QUS trends over the entire 60-hour time course of the study as well as the comparison between in vivo and ex vivo QUS outcomes.

Figure 3. Ex vivo mean AC and mean BSC estimates versus frequency for the pancreas in a rat model of cerulein-induced pancreatitis. Control = cage control. Saline = saline control. The numbers in parentheses represent the number of pancreases. AC, attenuation coefficient; BSC, backscatter coefficient.

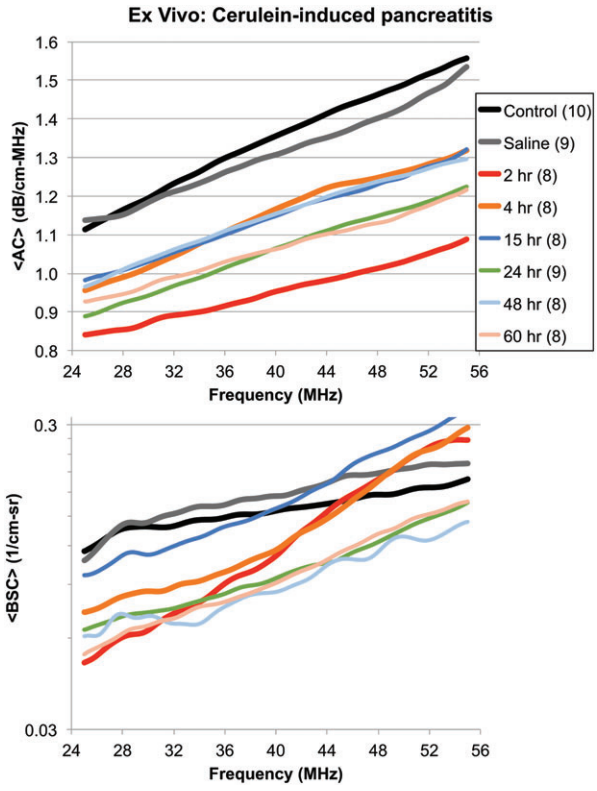

Histology

In the rat model of cerulein-induced pancreatitis, acinar cell vacuolation, autophagy, and apoptosis, with concomitant loss of zymogen and atrophy (shrinkage) as well as marked early interstitial edema and later infiltration by histiocytic macrophages, are prominent histomorphologic features.[11,12] Neutrophils are minor participants in the process in this protocol, and fibrosis is a late and not very prominent feature in this particular model.[18,21] Figure 5 illustrates these features at various time points after the last cerulein injection. Histologically, the cage and saline controls were the same. Mean histologic scores are summarized in Table 2.

Edema was an early and prominent change, being most severe at 2 hours and remained substantial, though somewhat lessened, through 48 hours after injection before declining to almost 0 by 60 hours. The marked edema at early time points is reflected in the increased pancreas weights noted in the 2-hour, 4-hour, and 15-hour time points (Table 1). This edema is a consistent feature of cerulein-induced pancreatitis and has been noted to occur after exposure to other secretagogue-mediated compounds as well, for example, cyanohydroxybutene.[27–29] Vacuolation was also a severe early change, peaking at 2 and 4 hours; like edema, it diminished with time and slowly declined to low levels by 60 hours. Autophagic vacuoles also appeared early and persisted through 48 hours, whereas apoptosis peaked at 4 hours, but, like autophagy, persisted through 48 hours. Zymogen was depleted throughout the entire course of the study, most severely so from 24 to 60 hours. Accompanying this was a decrease in acinar size, due to both decreased zymogen content and decreased numbers of acinar cells per acinus (loss from apoptosis). The

shrinkage of acini is also consistent with a steady decrease in pancreas weights over time through 60 hours, as acinar mass and cell numbers decreased. Histiocytes, as expected for these slow-moving leukocytes, were present in low numbers from 2 hours, reflective of the presence of resident tissue histiocytes, but increased substantially over time as recruitment from the bloodstream progressed, peaking at 60 hours. This is consistent with the model and reflects ingestion of apoptotic bodies and cellular debris in preparation for regeneration. Neutrophils, although present at all time points, were not prominent nor numerous, and evaluation scores were low, consistent with this rat model, where apoptosis rather than necroptosis or necrosis, predominates.[30] Fibrosis, as expected, was virtually absent in the early stages of pancreatitis, given that this is a "late" stage in the inflammatory response. Whereas very mild fibrosis was observed in a few pancreases at 24 hours, there was an increase subsequently, with the most being observed at 60 hours. Even so, by the criteria used, this did not involve more than 20% of the pancreatic capsular and interstitial area (data not shown), also consistent with this model.

The progression of changes observed in this study is reflective of the pathogenesis of cerulein-induced pancreatitis in the rat, in which hyperstimulation of pancreatic secretion leads to abnormal "trafficking" of zymogen granules with subsequent microautophagy (vacuole formation), macroautophagy (autophagic vacuoles), apoptosis, and subsequent "edematous" pancreatitis with histiocytic infiltration in response to the generation of apoptotic bodies.[16]

Figure 4. Ex vivo and in vivo AC and BSC estimates integrated over the frequency range 26–28 MHz for the pancreas in a rat model of cerulein-induced pancreatitis as a function of the time after cerulean injections. C = cage control. S = saline control. Error bar is the standard deviation. AC, attenuation coefficient; BSC, backscatter coefficient.

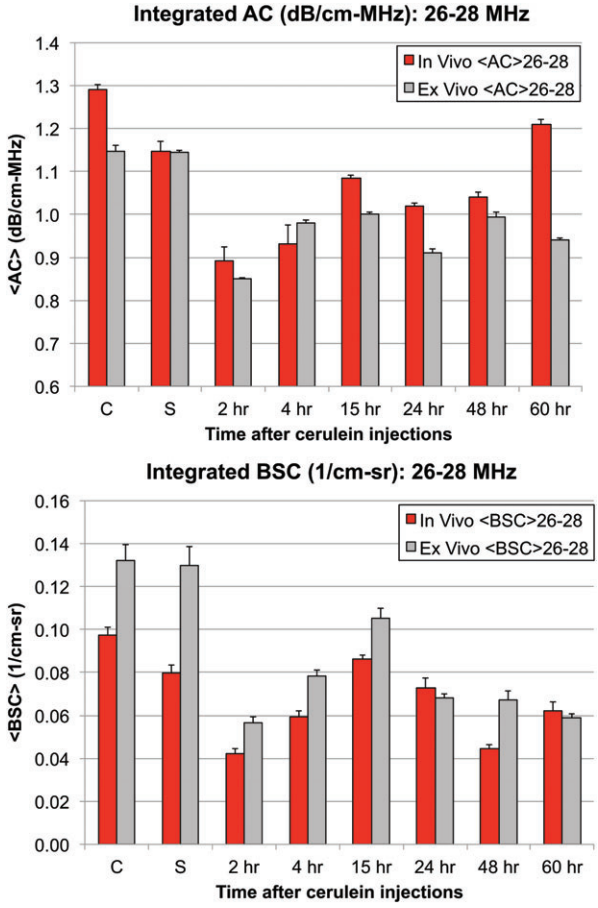

Figure 5. In all hematoxylin and eosin–stained pancreas images, thin arrows indicate apoptotic bodies (AB) while arrowheads indicate autophagic vacuoles (AV), asterisks indicate edema, and encircled areas enclose aggregates of histiocytes. The white bar in the lower right-hand corner of each image indicates 100 μm. (A) normal (cage control) pancreas showing densely packed acinar cells with abundant eosinophilic zymogen granules and sparse interstitium. (B) 2 hours after cerulean injection, illustrating severe interlobular edema with extensive acinar cell vacuolation, autophagy, and apoptosis. (C) 15 hours after cerulein injection, showing increased edema and early histiocyte infiltration but diminished acinar cell vacuolation; autophagy and apoptosis are still present. (D) 60 hours after cerulean injection, with intense histiocytic infiltration but greatly diminished autophagy, apoptosis, and vacuolation.

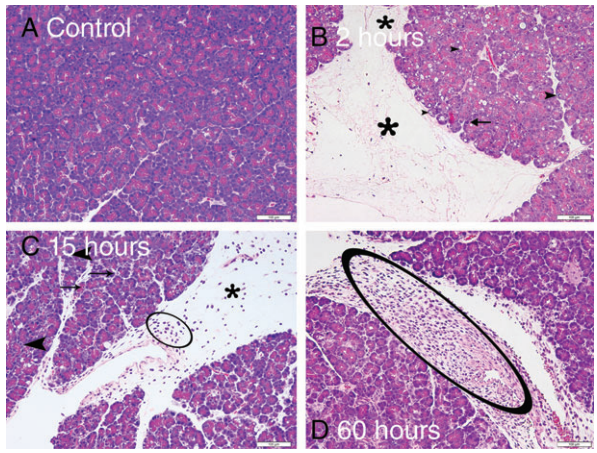

Table 2. Summary of Mean Histologic Scores

Time (h)	Zymogen Depletion (0–5)	Acinar Atrophy (0–5)	Vacuolation (0–5)	AV (0–5)	AB (0–4)	Edema (0–5)	Histiocytes (0–5)	PMNs (0–5)	Fibrosis (0–4)
0	0.0	0.0	0.0	0.0	0.0	0.0	0.0	0.0	0.0
2	2.5	2.1	4.5	2.3	0.6	4.5	1.4	1.1	0.0
4	1.6	1.8	4.4	3.1	2.3	2.0	1.3	1.0	0.0
15	2.4	1.7	2.8	1.6	1.6	2.8	1.3	1.0	0.3
24	3.7	3.0	2.1	2.2	1.7	1.9	3.7	1.2	0.8
48	3.0	2.3	1.6	1.6	2.6	2.8	2.8	1.6	1.6
60	3.6	4.3	1.4	0.5	0.9	0.1	4.4	1.3	3.1
Cage	0.0	0.0	0.0	0.0	0.0	0.0	0.0	0.0	0.0
Saline	0.0	0.0	0.0	0.0	0.0	0.0	0.0	0.0	0.0

AB, apoptotic body; AV, autophagic vacuole; PMNs, polymorphonuclear neutrophils.

With regard to QUS changes, the data suggest that interstitial edema and acinar cell vacuolation may be responsible for the changes in AC in this study because both would have an impact on attenuation of the signal as it passes through the affected tissue. For BSC, edema and vacuolation would have an impact on the BSC signal; however, as both waned over time, the closer association of cells and presence of apoptotic bodies may have increased the signal back toward control values. The subsequent decrease in BSC after 24 hours may reflect loss of cells from apoptosis and increased interstitium between the smaller acini containing acinar cells with sparse zymogen.

Conclusion

Quantitative ultrasound imaging is sensitive to tissue microstructure. The QUS biomarkers evaluated here, AC and BSC, can be measured using a routine clinical ultrasound scanner. Imaging of the pancreas could be added to an abdominal sonogram that has already been ordered for other suspected metabolic issues. Patients with nonspecific upper quadrant abdominal pain, nonspecific gastritis, or suspected gallstones could be imaged with ultrasound to rule out a pancreatic disorder. Quantitative ultrasound imaging could be used as a method to screen patients (general population or those at risk) for pancreatic disorders, following further research. Since pancreatitis and pancreatic cancer patients often present at the later stages of disease, early detection would be beneficial.

Understanding the progression of acute pancreatitis (as with early invasive pancreatic cancer) is imperative for successful intervention and early treatment in the progression of these diseases. The cerulein-induced model of acute pancreatitis in rats lends itself well to the study of AC and BSC biomarkers over time, as the degree of pancreatitis is mild and all animals survive, with pancreatitis resolving in approximately 7 days. This allows for the assessment of early reversible changes without progression to more severe changes such as necrosis; suppurative (neutrophilic) inflammation; and extensive, distortional fibrosis, masking these changes. Histologically, cerulein creates many types of morphologic changes that could potentially be detectable by QUS techniques.

Ultrasonically, we observed measurable effects in both AC and BSC relative to controls that reflect the effects over time of cerulein on tissue morphology, in particular interstitial edema and acinar cell vacuolation on AC and effects on BSC possibly reflective of not only edema but subsequent shrinkage and condensation of remaining acinar cells after edema resolves. This suggests that QUS biomarkers are sensitive enough to detect early changes in the pancreas during the earliest phases of acute pancreatitis. The general trend is decreased AC and BSC at early time points and then increases relative to controls (cage and saline) at later time points. Furthermore, at 2 hours after cerulean injection, the AC and BSC effects are significant, suggesting QUS detection limits may be even less than 2 hours. These results suggest a high likelihood for early detection of acute pancreatitis using QUS measures.

References

1. Carnovale A, Rabitti PG, Manes G, Esposito P, Pacelli L, Uomo G. Mortality in acute pancreatitis: is it an early or a late event? *J Pancreas* 2005; 6:438–444.
2. Perry AF, Dellon ES, Lund J, et al. Burden of gastrointestinal disease in the United States: 2012 Update. *Gastroenterology* 2012; 143:1179–1187.
3. SEER Cancer Statistics Factsheets: Pancreas Cancer. *National Cancer Institute website.* http://seer.cancer.gov/statfacts/html/pancreas.html. Accessed March 5, 2018.
4. Everhart JE. Cancer of the pancreas. In: Everhart JE (ed). *The Burden of Digestive Diseases in the United States.* Washington, DC: US Government Printing Office; 2008:61–64.
5. American Cancer Society. Cancer Statistics Center website. http://cancerstatisticscenter.cancer.org. Accessed March 5, 2018.
6. Everhart JE, Ruhl CE. Burden of digestive diseases in the United States. Part 1: Overall and upper gastrointestinal diseases. *Gastroenterology* 2009; 136:376–386.
7. Wallig MA, Sullivan JM. Exocrine pancreas. In: Haschek W, Rousseaux C, Wallig M (eds). *Haschek and Rousseaux's Handbook of Toxicologic Pathology.* 3rd ed. Waltham, MA: Elsevier; 2013:2361–2390.
8. Schottenfeld D, Beebe-Dimmer J. Chronic inflammation: a common and important factor in the pathogenesis of neoplasia. *CA Cancer J Clin* 2006; 56:69–83.
9. Wilson JS, Pirola RC, Apte MV. Stars and stripes in pancreatic cancer: role of stellate cells and stroma in cancer progression. *Front Physiol* 2014; 5:1–11.
10. Willemer S, Elsaesser HP, Adler G. Hormone-induced pancreatitis. *Eur Surg Res* 1992; 24(suppl. 1):29–39.
11. Zhang J, Rouse RL. Histopathology and pathogenesis of caerulein-, duct ligation-, and arginine-induced acute pancreatitis in Sprague-Dawley rats and C57BL6 mice. *Histol Histopathol* 2014; 29:1135–1152.
12. Usborne AL, Smith AT, Engle SK, Watson DE, Sullivan JM, Walgren JL. Biomarkers of exocrine pancreatic injury in 2 rat acute pancreaititis models. *Toxicol Pathol* 2014; 42:195–203.
13. De Caro G, Endean R, Erspamer V, Roseghini M. Occurrence of caerulein in extracts of the skin of *Hyla caerulea* and other Australian hylids. *Br J Pharmacol Chemother* 1968; 33:48–58.
14. Johnson LR, Stening GF, Grossman MI. Effect of sulfation on the gastrointestinal actions of caerulein. *Gastroenterology* 1970; 58: 208–216.
15. Gaisano HY, Gorelick FS. New insights into the mechanisms of pancreatitis. *Gastroenterology* 2009; 136:2040–2044.
16. Zhang L, Zhang J, Shea K, et al. Autophagy in pancreatic acinar cells in caerulein-treated mice: Immunolocalization of related proteins and their potential as markers of pancreatitis. *Toxicol Pathol* 2014; 42:435–457.
17. Mareninova OA, Hermann K, French SW, et al. Impaired autophagic flux mediates acinar cell vacuole formation and trypsinogen activation in rodent models of acute pancreatitis. *J Clin Invest* 2009; 119:3340–3355.
18. Hyun JJ, Lee HS. Experimental models of pancreatitis. *Clin Endosc* 2014; 47:212–216.
19. Wang Y, Kayoumu A, Lu G, et al. Experimental models in Syrian golden hamster replicate human acute pancreatitis. *Sci Rep* 2016; 6:1–8.
20. Renner IG, Wisner JR Jr. Ceruletide-induced acute pancreatitis in the dog and its amelioration by exogenous secretin. *Int J Pancreatol* 1986; 1:39–49.
21. Su KH, Cuthbertson C, Christophi C. Review of experimental animal models of acute pancreatitis. *HPB* 2006; 8:264–286.
22. Elsässer HP, Adler G, Kern HF. Time course and cellular source of pancreatic regeneration following acute pancreatitis in the rat. *Pancreas* 1986; 1:421–429.
23. Yao LX, Zagzebski JA, Madsen EL. Backscatter coefficient measurements using a reference phantom to extract depth-dependent instrumentation factors. *Ultrason Imaging* 1990; 12:58–70.
24. Han A, Andre MP, Erdman JW Jr, Loomba R, Sirlin CB, O'Brien WD Jr. Repeatability and reproducibility of a clinically based QUS phantom study and methodologies. *IEEE Trans Ultrason Ferroelectr Freq Control* 2017; 64:218–231.
25. Han A, Abuhabsah R, Miller RJ, Sarwate S, O'Brien WD Jr. The measurement of ultrasound backscattering from cell pellet biophantoms and tumors ex vivo. *J Acoust Soc Amer* 2013; 134: 686–693.
26. Chen X, Phillips D, Schwarz KQ, Mottley JG, Parker KJ. The measurement of backscatter coefficient from a broadband pulse-echo system: A new formulation. *IEEE Trans Ultrason Ferroelectr Freq Control* 1997; 44:515–525.
27. Wallig MA, Gould DH, Fettman MJ. Selective pancreatotoxicity in the rat induced by the naturally occurring plant nitrile, 1-cyano-2-hydroxy-3-butene. *Food Chem Toxicol* 1988; 26:137–147.
28. Maher M, Chernenko G, Barrowman JA. The acute pancreatotoxic effects of the plant nitrile 1-cyano-2-hydroxy-3-butene. *Pancreas* 1991; 6:168–174.
29. Walgren JL, Mitchell MD, Whiteley LO, Thompson DC. Evaluation of two novel peptide safety markers for exocrine pancreatic toxicity. *Toxicol Sci* 2007; 96:184–193.
30. Mareninova OA, Sung KF, Hong P, et al. Cell death in pancreatitis: Caspases protect from necrotizing pancreatitis. *J Biol Chem* 2006; 281:3370–3381.